Fabrication and Characterization of an Upside-Down Carbon Nanotube Microelectrode Array

Gaio, Nikolas; Silvestri, Cinzia; van Meer, Berend; Vollebregt, Sten; Mummery, CL; Dekker, Ronald

DOI
10.1109/JSEN.2016.2573854

Publication date
2016

Document Version
Accepted author manuscript

Published in
IEEE Sensors Journal

Fabrication and characterization of an Upside-down Carbon Nanotube (CNT) Microelectrode array (MEA)

Nikolas Gaio[1,*], Cinzia Silvestri[1], Berend van Meer[2], Sten Vollebregt[1], Christine L. Mummery[2], Ronald Dekker[1]

Abstract

Microelectrode arrays (MEAs) are widely used in biological application to locally stimulate and record the electrical activity of living cells. Here, a novel fabrication process for a carbon nanotube (CNT) based MEA integrated on the backside of a free standing stretchable membrane is reported. The new process flow overcomes the manually intensive procedures used in previous works. The microfabricated upside-down CNT MEA consists of microelectrodes with an area of $110\,\mu m^2$ covered with Cobalt-grown CNTs. The surface area enhancement and the foam-like morphology of the CNTs allows an increase of the charge injection per unit area at the electrode-electrolyte interface, resulting in a significantly lower electrochemical impedance of the electrodes. In particular, at 1 kHz the fabricated CNT-MEA electrodes show a reduction of the overall impedance up to 96% in comparison to benchmark TiN electrodes. The obtained results confirm the effectiveness of the proposed surface texturing through CNT integration. Moreover, the quality and morphology as well as the biocompatibility of the fabricated CNT-based electrodes were assessed. The obtained results demonstrate that significant improvement can be achieved by integrating structured nanoporous material on MEAs.

An earlier version of this paper was presented at the 2015 IEEE Sensor Conference and was published in its Proceedings.
http://ieeexplore.ieee.org/stamp/stamp.jsp?arnumber=7370350
[1]Laboratory of Electronic components, Technology & Materials (ECTM), EKL, Delft University of Technology
[2]Department of Anatomy and Embryology, Leiden University Medical Center, the Netherlands

Fabrication and characterization of an Upside-down Carbon Nanotube (CNT) Microelectrode array (MEA)

I. Introduction

MICRO-ELECTRODE arrays (MEAs) are widely employed to monitor and stimulate *in vitro* and *in vivo* biological systems composed of electrically active cells e.g. neurons or cardiomyocytes [1]–[5]. In order to analyze these complex systems with a sufficiently high spatial resolution, the electrodes need to have a relatively small geometric surface area (GSA). However, while the storage charge capacity of the electrode is proportional to the GSA, the overall electrochemical impedance reduces, resulting in a high noise levels when subcellular scale electrodes are used. Moreover, during high current density stimulation small electrodes can experience electrochemical instabilities that can result in device and tissue damage [6].

Electrode materials can be divided into Faradaic or capacitive depending on the reactions at the electrode-electrolyte interface. By coating the electrode with Faradaic materials, e.g. activated iridium oxide films (AIROF) [7] or sputtered iridium oxide [8], high levels of charge injection per unit area at the electrode-electrolyte interface can be obtained which improves the electrodes electrochemical performance. The main disadvantage of these materials is that cell monitoring and stimulation are based on redox reactions at the electrode-electrolyte interface. These are usually undesirable, since they imply the creation and consumption of chemical species which could eventually affect the cell culture [9].

Capacitive coatings are a more suitable option for applications involving cell activity monitoring. Unlike Faradaic materials, the charge injection of these coatings is based on ion displacement on top of the electric double layer found at the electrode-electrolyte interface. However, to provide the same charge injection capacity as Faradaic reactions, capacitive coatings need to have a porous micro-pattern which increases the specific surface area (SSA) of the electrode. Examples of these type of coatings are fractal Titanium Nitride (TiN) and carbon nanotubes (CNTs) [9]. Previous work [6] has shown how CNT coatings can drastically improve the SNR of the recorded cell potential by increasing double-layer charge capacity as a consequence of their high SSA/GSA ratio. Furthermore, CNTs provide additional advantages such as high mechanical and electrical stability [10], good electrical conductance [10], and stable cell-electrode coupling [11].

However, CNTs cannot be easily grown on surfaces made of common biocompatible polymers like PDMS etc., due to the high thermal budget required for their synthetization. For this reason, standard CNT MEAs are usually fabricated on rigid supports, e.g. Silicon (Si) wafers. Consequently, CNT MEAs cannot be employed in applications like brain stimulators [6] and Organ-on-Chips devices [12], where the MEA needs to be integrated on a stretchable or a flexible surface.

This problem has been overcome by first growing and patterning the CNT electrodes on a rigid Si substrate, and then transferring them onto a flexible/stretchable polymer film, followed by a partial isolation with a second film [13]. However, this process contains intensive manual procedures that may drastically reduce the device yield.

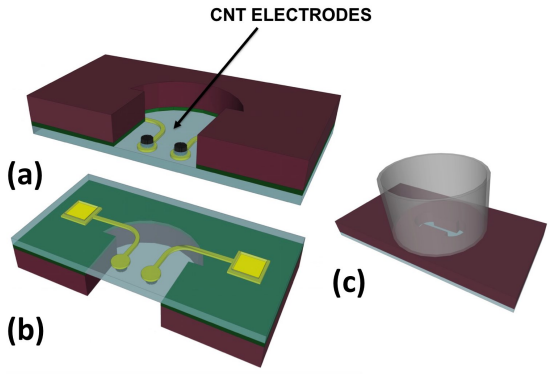

Fig. 1. 3D sketch of upside-down CNT MEA: (a) backside and (b) frontside. The MEA consists of 12 circular electrodes (diameter: 12 µm) covered with Co-grown CNTs (height: 1 µm). (c) MEA with glued plastic cylinder on die backside.

This work reports a novel fabrication process to embed CNT MEAs in polymer membranes, in which no manual assembly and sample handling are required. Like in [13], the polymer membrane is deposited after CNT growth, however, in our case the electrodes are released by etching the support Si wafer from the backside rather than peeling off the membrane. Fig. 1 shows a schematic rendering of the final device, called the upside-down CNT MEA. The concept is validated with the fabrication and the complete characterisation of a prototype upside-down CNT MEA embedded on the backside of a rigid membrane.

II. MEA Micro-fabrication

In this work, besides the upside-down CNT MEA, two other benchmark MEAs were fabricated: a *standard* TiN MEA and a *standard* CNT MEA. In all cases the devices

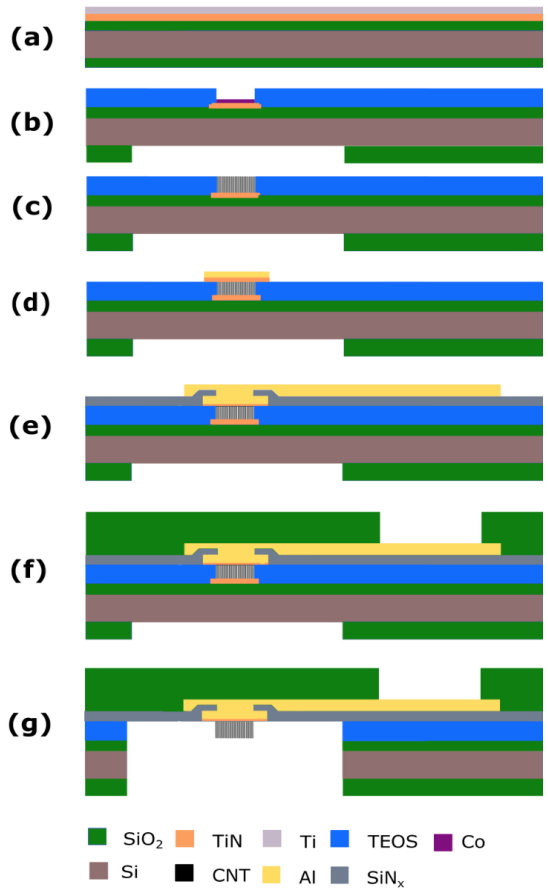

Fig. 2. Process flow of the upside-down CNT MEA: a) Ti/TiN/Ti stack (5/50/100 nm); b) hole array etching and Co evaporation and patterning; c) CNT growth; d) metal lids fabrication made of TiN and Al; e) metal lines sputtering and etching; f) membrane definition and contact pads opening; e) membrane releasing. Figure not on scale.

were fabricated starting with 100 mm-diameter polished monocrystalline silicon (Si) wafers (525 µm thickness).

A. Upside-down CNT MEA

The upside-down CNT MEA consists of a 12 µm thick membrane provided with CNT based electrodes (Fig. 1 a-b). The electrodes are connected to Aluminum (Al) interconnects embedded in the membrane. The processing starts by growing 2 µm of thermal oxide. Then a layer stack consisting of 5 nm of Titanium (Ti), 50 nm of Titanium Nitride (TiN) and 100 nm of Ti is sputter deposited (Fig. 2 a). The purpose of the Ti bottom layer is to improve the adhesion between the TiN and the SiO_2, while the TiN layer acts as support layer for the CNT growth.

On top of the Ti/TiN/Ti stack a 1 µm thick layer of Tetraethyl Orthosilicate (TEOS) is deposited. The TEOS layer is patterned using reactive ion etching (RIE) to define an array of holes with a depth of 1 µm and 12 µm in diameter, landing on the Ti/TiN/Ti disks (Fig. 2 b). The top Ti layer prevents the fluorine-chemistry plasma, used to etch the TEOS layer, from entering in contact with the TiN support layer and affecting CNT alignment [14]. The 100 nm Ti layer is subsequently removed by soaking the wafer in a Hydrofluoric acid (HF) solution.

Next, a 5 nm thick layer of Cobalt (Co) is evaporated in the cavities to catalyze the CNT growth (Fig. 2b). The enclosed CNTs are grown by low-pressure chemical vapor deposition (LPCVD) at 500°C for 38 seconds reaching an height of 1 µm (Fig. 2 c). The growth temperature is chosen to have both adequate CNT alignment as well as CMOS compatibility. More details can be found in the CNTs characterization section. After growing the CNTs, the CNT tips are covered with a metal lids consisting of 100 nm TiN and 1 µm Al (Fig. 2 d).

The last process sequence is the fabrication of the membrane that embeds the metal lines connecting the CNT electrodes to the contact pads (Fig. 2 e). This membrane can be either a PDMS-based stretchable membrane [12], or a rigid membrane consisting of a stack of 2 µm plasma-enhanced CVD (PECVD) Silicon Nitride (Si_3N_4) and 10 µm of PECVD SiO_2 (this work) (Fig. 2 f). The membrane release process starts by etching through the wafer from the backside by deep reactive-ion etching (DRIE) and landing on the SiO_2 layer, and ends by etching the remaining layer in buffered Hydrofluoric Acid (BHF) (Fig. 2 g). The TiN disks embedded in the SiO_2 detach from CNT roots during the BHF etching.

B. Standard MEAs

The fabrication of the reference MEA device starts by growing 2 µm of thermal SiO_2 (Fig. 3 a). Metal lines, contact pads and electrodes are fabricated by deposition and patterning of 100 nm of TiN, 500 nm of Ti and 50 nm of TiN (Fig. 3 b). The metal lines are isolated with a 1 µm thick TEOS layer, which is subsequently dry etched to open electrodes and contact pads (Fig. 3 c). This is the last process step of the standard TiN electrodes. The fabrication of the

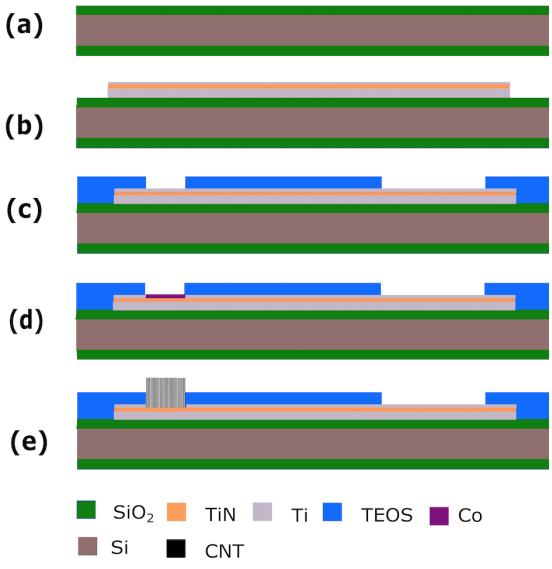

Fig. 3. Process flow for the standard MEAs: a) SiO_2 growth; b) deposition and patterning of Ti/TiN/Ti stack; c) deposition and patterning of TEOS layer to define electrodes and contact pads; d) Co deposition and patterning; e) CNT growth. Figure not on scale.

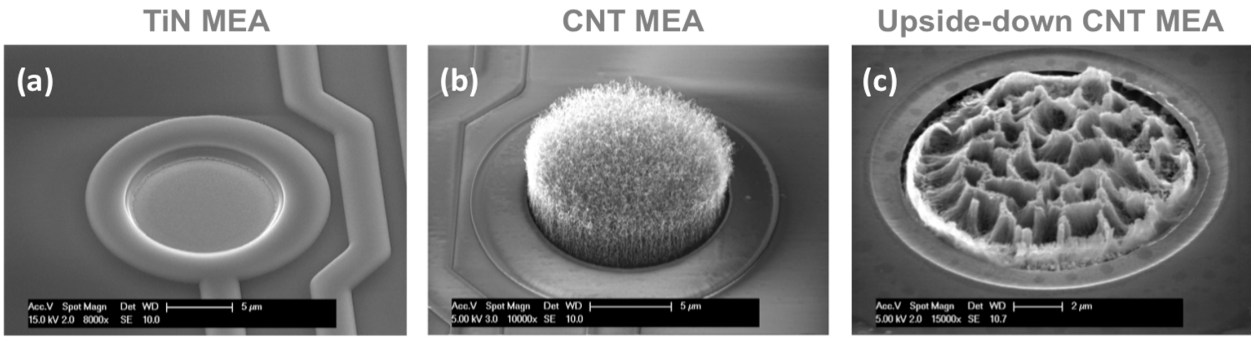

Fig. 4. SEM pictures of the fabricated electrodes: (a) standard TiN electrode, (b) standard CNT electrode (not affected by CNT buckling) and (c) upside-down CNT electrode (showing severe CNT buckling due to BHF etching).

standard CNT MEA continues with the evaporation and patterning of 5 nm of Co and by growing the CNTs (Fig. 3 d-e).

Fig. 4 shows top view scanning electron microscopy (SEM) images of all three types of fabricated MEAs. The BHF etching, performed as the last fabrication step in the upside-down CNT MEA, provokes a buckling phenomenon of the CNT arrays. Consequently, the GSA of the CNT array is reduced, affecting the final device performance (Fig. 4 c).

III. CNTs and MEAs Characterization Procedure

The combination of the barrier and catalyst layers is essential requirement for the growth of vertically aligned carbon nanotubes using LPCVD. The CNT morphology and quality crucially depends on the composition of these two layers. Although different barrier materials and catalyst nanoparticles have been reported in literature [15], [16], one of the aims of this work was to maintain CMOS compatibility to allow for wafer-scale integration and transfer of the process to standard foundries. These lead us to combine TiN and Co nanoparticles as barrier and catalyst layers, respectively. In particular, Co guarantees CMOS compatibility due to the lower diffusion coefficient compared to Cu and Fe, while additionally it does not result in deep-level traps in Si.

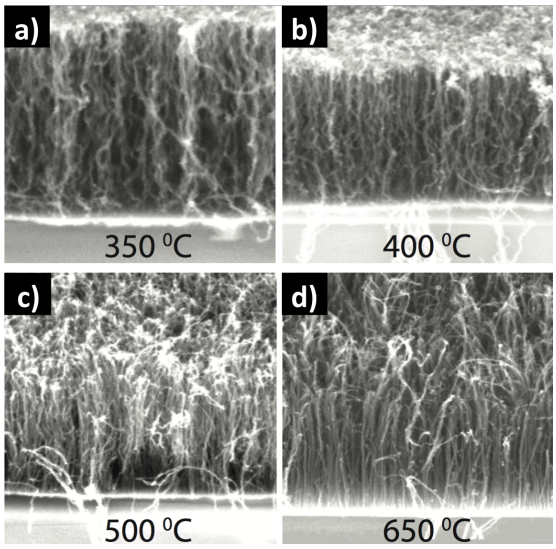

Fig. 5. CNT forests grown at (a) 350°C, (b) 400°C, (c) 500°C and (d) 650°C. Higher growth temperatures showed higher CNT alignment but lower uniformity.

As mentioned before, the growing of the CNTs was performed by LPCVD in a commercial deposition system (AIXTRON Blackmagic). Briefly, after loading the wafer in the reactor, the entire system is pumped down to < 0.1 mbar. 700 sccm of Hydrogen (H_2) are then injected into the reactor, while the temperature and pressure are ramped to 500°C and 80 mbar, respectively. This step is followed by a three minutes anneal to pre-heat the chamber to the required deposition temperature. Next 50 sccm of Acetylene (C_2H_2) are added and the CNTs are synthesized on top of the catalyst particles. A more detailed description of the CNT deposition process can be found elsewhere [17].

A. CNT quality and morphology

The morphology and quality of CNT dense arrays are strongly dependent on the deposition temperature. In this work, four different temperatures have been investigated: 350, 400, 500 and 650°C. 350°C is an extremely low temperature for CNT growth by CVD but very attractive from a standpoint of CMOS compatiblity. In fact, the low activation energy of the Co catalyst (0.4-0.43 eV) allows a low temperature process while achieving a sufficient growth rate [17]. To determine the dependence of the growth rate from the process temperature, a sequences of time-progressive images taken at different deposition times are analyzed by SEM. Growth rates of 0.285, 1.977, 30.83, 163 nm/sec for 350, 400, 500 and 650°C, respectively, were achieved.

A widely used technique to assess CNT quality is Raman spectroscopy. The spectral response of all samples, with a spectra coverage of 3550 cm^{-1}, was recorded through a Renishaw inVia Raman spectroscope with 514 nm laser wavelength. For each sample three Raman spectra were acquired to ensure high measurement accuracy. Moreover, to determine whether the Co nanoparticles are lifted up (tip-growth mechanism) or pinned down (root-growth mechanism), a double temperature growth test has been performed [18]. The first step consists of 2 minutes CNT growth at

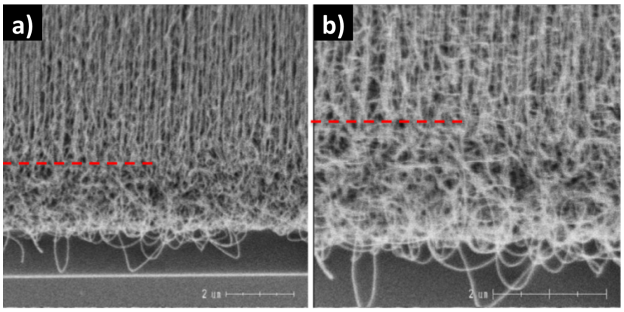

Fig. 6. SEM images showing the results obtained from the double temperature growth test. The red dotted line identifies the two different synthesis phases. Underneath the line, CNT are grown for 2 minutes at 500°C and above the line at 600°C for other 2 minutes. (b) Close up on the achieved CNT morphology.

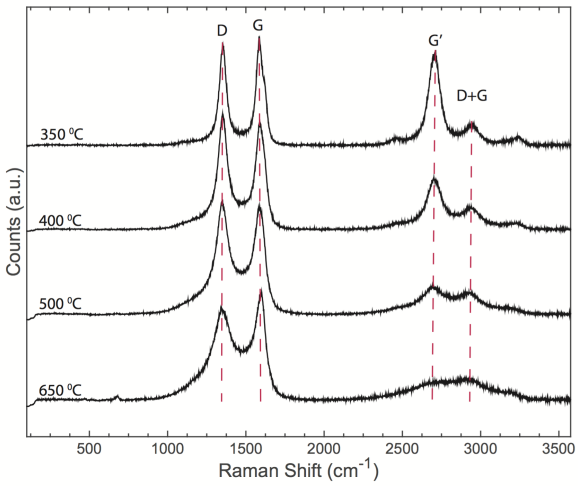

Fig. 7. Raman spectra of CNTs grown on 5 nm Co at four different growth temperatures. To obtain insights about CNT properties like purity and structural quality, the ($I_{D/G}$) ratio is calculated. The ($I_{D/G}$) ratio decreases as the CNT growth temperature increases.

500°C; then the second step is performed by increasing the reactor temperature up to 600°C and let the CNT growing for another 2 minutes.

B. Biocompatibility assessment

The biocompatibility of the Co-grown CNTs were tested by plating human pluripotent stem cell derived cardiomyocytes on top of the CNT forests. Co-grown CNT samples were sterilized in ethanol and then coated with Matrigel (Invitrogen) to induce cell attachment. Next, the cells were plated and cultured on the CNT samples for 3 days in a CO_2 incubator at 37°. The cells were then fixed using 2% paraformaldehyde for 30 minutes and stained with an anti-alpha-actinin antibody and 4,6-diamidino-2-phenylindole (DAPI) to reveal the sarcomeric structures and cell nucleus, respectively.

C. Electrochemical tests

The electrochemical performance of all MEAs was characterized by electrochemical impedance spectroscopy (EIS) in a phosphate buffered saline (PBS) solution. In order to perform EIS on both the standard electrodes and the upside-down devices, plastic cylinders were glued to the surface of the device (Fig. 1 c). These cylinders were used to contain the PBS solution during electrochemical characterization, and to guarantee complete isolation of the solution from the device metal pads. An Ag/AgCl electrode and a platinum strip were used as reference and counter electrode, respectively. The EIS tests were performed with an Autohom Metrolab potentiostat with FRA2 module. The amplitude of potential variations between working and reference electrode was equal to 20 mV. The output current signal has been checked during measurements to detect eventual non-linearities caused by high-amplitude stimulations.

IV. Results and Discussion

A. CNT Biocompatibility and quality assessment

Fig. 5 shows the SEM images of 1 µm long CNTs grown at different temperatures. A careful inspection of the obtained morphologies indicates that CNTs grown at 650°C showed a better alignment compared to the ones synthesized at lower temperatures. However, higher growth temperatures result in less uniformity in height across the CNT forest (Fig. 5 c-d). CNTs grown at 350°C and 400°C showed a similar morphology.

Fig. 6 shows the result obtained from the double temperature growth test. As highlighted by the red dotted line, CNTs grown at two different temperature present two distinct phases: the top segment of the CNT forest, grown at 600°C, is well aligned as opposed to the bottom one, grown at lower temperature (500°C). In contrast to what is claimed in [17], these results demonstrate that the employed catalyst/support combination implies a tip-growth process. This is probably due to a weak interaction between TiN surface and Co particles. Moreover, the tip-growth mechanisms implies that Co nanoparticles are enclosed in the TiN/Al during the metallization step described in Section

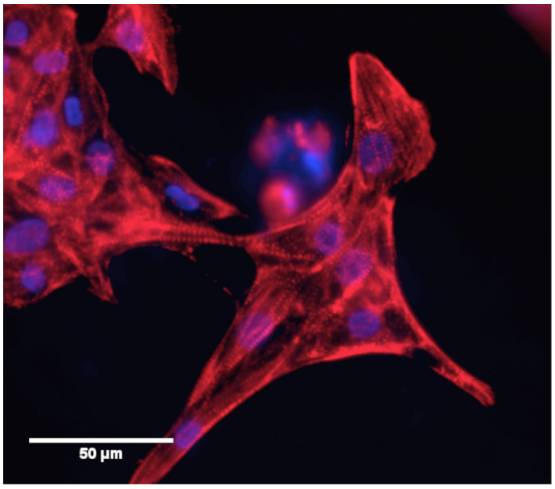

Fig. 8. Merged fluorescent images of fixed human stem cells derived cardiomyocytes plated in on top of CNTs for 3 days: nucleus are stained in blue (stain: DAPI) and alpha-actinin in red (stain: CY3).

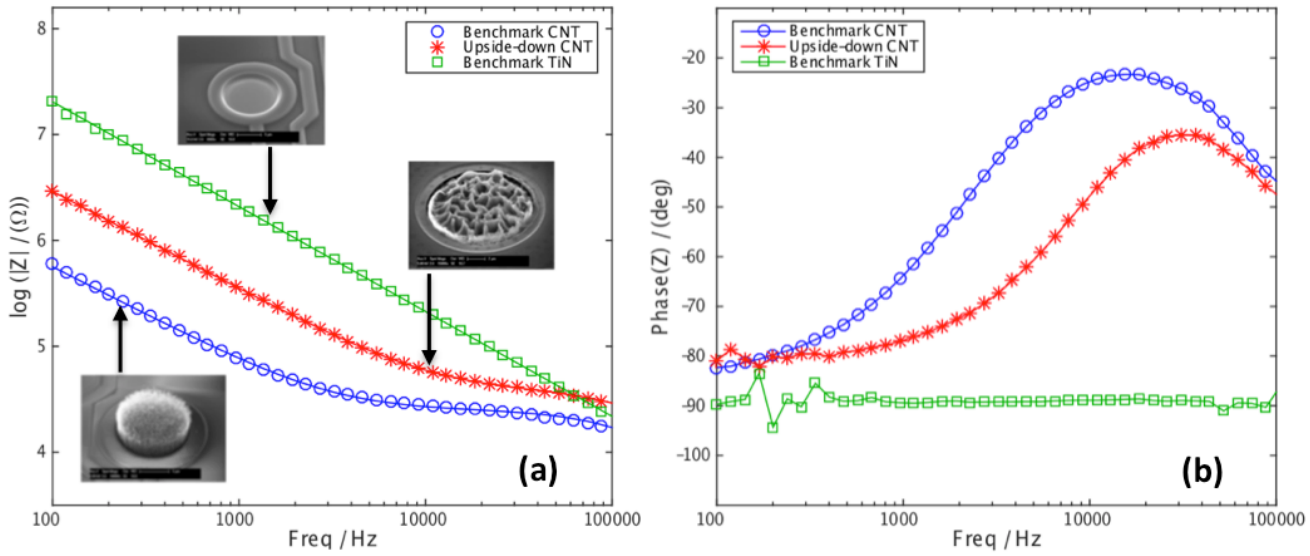

Fig. 9. (a,b) Bode plot ((a) amplitude and (b) phase) of impedance spectra of a standard CNT electrode (not affected by CNT buckling), an upside-down CNT electrode and a standard TiN electrode ($110\,\mu m^2$ geometric surface area). EIS at 1 kHz are equal to 2.2 MΩ, 240 kΩ and 87 kΩ for benchmark CNT, upside-down CNT and benchmark TiN, respectively.

II-A.

Fig. 7 shows the first and second order bands of Raman spectrum obtained from CNT forests grown at different temperatures. The spectra deconvolution was made with a combination of eight Lorentzian and two Gaussian distributions [17]. The obtained ratio between the amplitudes of the D and G peaks ($I_{D/G}$) is equal to 1.11, 1.14, 1.27 and 1.02 for the CNTs grown at 350, 400, 500 and 650°C, respectively. The $I_{D/G}$ ratio of the CNTs grown at 350° reveals a crystallinity degree comparable to the ones reported in other works [11], in which the CNT growth temperature was even higher.

With respect to CNT biocompatibility, after three days the stem cell derived cardiomyocytes plated on the CNT electrodes were beating spontaneously, demonstrating their viability and functionality. In Fig. 8 a fluorescent image of the cells on the CNTs is shown. The cells exhibit characteristic striated sarcomeric structures found in functional cardiomyocytes. This demonstrates the short term biocompatibility of CNTs for culturing stem cell derived cardiomyocytes.

B. Electrochemical characterization results

The EIS spectra of a representative electrode of the upside-down CNT MEA are shown in Fig. 9 a and b. The impedance amplitude and phase over the investigated frequency range are compared to the standard TiN electrode. In particular, at 1 kHz the upside-down CNT electrode revealed a marked impedance reduction, one order of magnitude, compared to a flat TiN electrode: 240 kΩ and 2.2 MΩ, respectively (Fig. 9 a). However, the previously observed CNT buckling phenomenon severely affects the upside-down CNT MEA impedance. In fact, the standard CNT electrodes, which are not affected by buckling, outperform in comparison to the upside-down MEAs. At 1 kHz the unbuckled CNT electrodes have an impedance as low as 87 kΩ. The measured TiN electrodes showed a constant phase behaviour in the investigated frequency range as an ideal smooth capacitive electrode [9]. On the contrary, the standard and the upside-down CNT electrodes showed a similar curvilinear phase angle trend induced by their porosity. The shift between these two spectra relies on the different GSA as observed by others [1].

The correlation between CNT buckling and the resulting impedance increase has been further studied by inducing the phenomenon on a CNT standard electrode. The standard CNT MEA was covered with isopropyl alcohol (IPA) for 5 minutes and then rinsed with PBS for 3 times. Fig. 10 a-b show a SEM image of a CNT forest before and after IPA treatment. As shown, IPA causes the same buckling effect induced by BHF. In particular, the impedance amplitude of the CNT electrodes increased from 87 kΩ up to 367.1 kΩ at 1 kHz after IPA treatment, demonstrating that CNT buckling severely

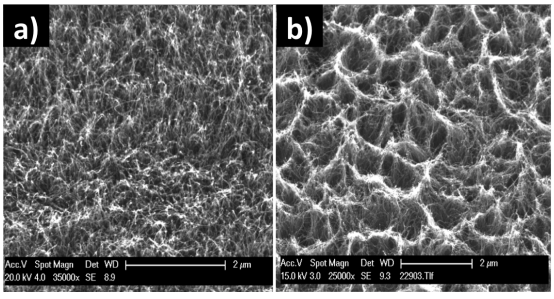

Fig. 10. IPA effects on 1 µm high CNT forest. In particular, (a) before and (b) after the IPA treatment.

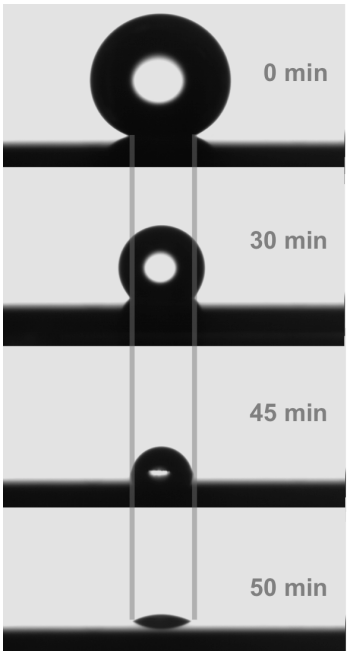

Fig. 11. Evaporation process of a 7 µL drop of water deposited on top of a CNT forest. The contact area between water and CNTs remains pinned, as indicated by the two vertical lines, while the contact angle is reduced strongly (decreasing from 150°, measured at the initial time, to 25° after 50 minutes).

affects the electrochemical performance of CNT electrodes. Therefore, to overcome the limitation presented in the upside-down CNT electrodes it is necessary to prevent or reduce the CNT buckling. A valuable option is to make use of HF vapor etching for the CNT electrode release instead of conventional BHF etching.

The reported impedance values were recorded waiting 30 minutes after immersion in the PBS solution. In fact, during standard CNT MEA characterization a remarkable drop in impedance is observed as time passes: from 160 kΩ right after the PBS immersion to 87 kΩ after 30 minutes. This variation is connected to the wettability transition phenomenon occurring in the CNT forest, called Cassie-Baxter to Wenzel transition [19].

To verify if a wettability transition occurs on the CNT forest, the hydrophobicity of the Co-grown CNTs was monitored. Data was collected by measuring the contact angle and the contact area of the droplet on top of the CNT forest as a function of time. As shown in Fig. 11, during water evaporation the contact line remains pinned while the contact angle decreases, proving that the water is penetrating into the CNT forest voids [19]. By taking advantage of this phenomenon, it is possible to reduce the electrochemical impedance of a MEA without any plasma treatment, known to deteriorate CNT conductivity. In fact, the obtained impedance value is in the same order of magnitude of a similar CNT MEA subjected to plasma treatment [6].

V. Conclusion

A novel fabrication process has been presented to embedded CNT microelectrode arrays (MEA) on the backside of a polymer membrane. In contrast to previously reported fabrication schemes, the newly presented procedure completely avoids manual assembly, such as membrane peeling and alignment, and thereby increases device reliability and yield, while at the same time it opens the route towards high-volume production. The fully automated procedure has been tested by fabricating the upside-down CNT MEA on a SiN membrane.

By using EIS, the impedance response of different MEAs was measured. The increase of the electrode surface area with CNTs resulted in an impedance reduction of up to 96% at 1kHz, compared to standard TiN electrodes. Moreover, the morphology and quality of CNT forests grown at different process temperature were investigated. It can be concluded that CNTs grown at 500°C represent the best compromise between quality, packing density, surface to volume ratio and thermal budget. However, the possibility to lower the temperature to 350°C to make the entire process more CMOS compatible is still a valuable option. Finally, the biocompatibility of the CNT electrodes was assessed by plating human pluripotent stem cell-derived cardiomyocytes.

The upside down CNT fabrication method presented in this paper enables the high-volume production of stretchable MEA devices with low impedance CNT electrodes.

Acknowledgment

The authors gratefully acknowledge the technical support and advice of the staff at the Else Kooi Laboratory (EKL). This work was performed in the framework of the ECSEL JU InForMed Project (grant no. 2014-2-662155).

References

[1] H.-B. Zhou, G. Li, X.-N. Sun, Z.-H. Zhu, Q.-H. Jin, J.-L. Zhao, and Q.-S. Ren, "Integration of au nanorods with flexible thin-film microelectrode arrays for improved neural interfaces," *Microelectromechanical Systems, Journal of*, vol. 18, no. 1, pp. 88–96, 2009.

[2] D. E. Arreaga-Salas, A. Avendaño-Bolívar, D. Simon, R. Reit, A. Garcia-Sandoval, R. L. Rennaker, and W. Voit, "Integration of high-charge-injection-capacity electrodes onto polymer softening neural interfaces," *ACS applied materials & interfaces*, vol. 7, no. 48, pp. 26 614–26 623, 2015.

[3] L. Wang, L. Liu, X. Li, N. Magome, K. Agladze, and Y. Chen, "Multi-electrode monitoring of guided excitation in patterned cardiomyocytes," *Microelectronic Engineering*, vol. 111, pp. 267–271, 2013.

[4] I. Kehat, L. Khimovich, O. Caspi, A. Gepstein, R. Shofti, G. Arbel, I. Huber, J. Satin, J. Itskovitz-Eldor, and L. Gepstein, "Electromechanical integration of cardiomyocytes derived from human embryonic stem cells," *Nature biotechnology*, vol. 22, no. 10, pp. 1282–1289, 2004.

[5] S. Rajaraman, S.-O. Choi, M. A. McClain, J. D. Ross, M. C. LaPlaca, and M. G. Allen, "Metal-transfer-micromolded three-dimensional microelectrode arrays for in-vitro brain-slice recordings," *Microelectromechanical Systems, Journal of*, vol. 20, no. 2, pp. 396–409, 2011.

[6] K. Wang, H. A. Fishman, H. Dai, and J. S. Harris, "Neural stimulation with a carbon nanotube microelectrode array," *Nano letters*, vol. 6, no. 9, pp. 2043–2048, 2006.

[7] S. F. Cogan, P. R. Troyk, J. Ehrlich, and T. D. Plante, "In vitro comparison of the charge-injection limits of activated iridium oxide (airof) and platinum-iridium microelectrodes," *Biomedical Engineering, IEEE Transactions on*, vol. 52, no. 9, pp. 1612–1614, 2005.

[8] S. F. Cogan, T. Plante, and J. Ehrlich, "Sputtered iridium oxide films (sirofs) for low-impedance neural stimulation and recording electrodes," in *Engineering in Medicine and Biology Society, 2004. IEMBS'04. 26th Annual International Conference of the IEEE*, vol. 2. IEEE, 2004, pp. 4153–4156.

[9] S. F. Cogan, "Neural stimulation and recording electrodes," *Annu. Rev. Biomed. Eng.*, vol. 10, pp. 275–309, 2008.

[10] L. Bareket-Keren and Y. Hanein, "Carbon nanotube-based multi electrode arrays for neuronal interfacing: progress and prospects," *Frontiers in neural circuits*, vol. 6, 2012.
[11] A. O. Fung, C. Tsiokos, O. Paydar, L. H. Chen, S. Jin, Y. Wang, and J. W. Judy, "Electrochemical properties and myocyte interaction of carbon nanotube microelectrodes," *Nano letters*, vol. 10, no. 11, pp. 4321–4327, 2010.
[12] S. K. Pakazad, A. Savov, A. Van de Stolpe, and R. Dekker, "A novel stretchable micro-electrode array (smea) design for directional stretching of cells," *Journal of Micromechanics and Microengineering*, vol. 24, no. 3, p. 034003, 2014.
[13] M. David-Pur, L. Bareket-Keren, G. Beit-Yaakov, D. Raz-Prag, and Y. Hanein, "All-carbon-nanotube flexible multi-electrode array for neuronal recording and stimulation," *Biomedical microdevices*, vol. 16, no. 1, pp. 43–53, 2014.
[14] S. Vollebregt, R. Ishihara, J. Derakhshandeh, J. van der Cingel, H. Schellevis, and C. Beenakker, "Integrating low temperature aligned carbon nanotubes as vertical interconnects in si technology," in *Nanotechnology (IEEE-NANO), 2011 11th IEEE Conference on*. IEEE, 2011, pp. 985–990.
[15] C. Silvestri, B. Morana, G. Fiorentino, S. Vollebregt, G. Pandraud, F. Santagata, G. Q. Zhang, and P. M. Sarro, "Cnt bundles growth on microhotplates for direct measurement of their thermal properties," in *Micro Electro Mechanical Systems (MEMS), 2014 IEEE 27th International Conference on*. IEEE, 2014, pp. 48–51.
[16] W. Zhou, Z. Han, J. Wang, Y. Zhang, Z. Jin, X. Sun, Y. Zhang, C. Yan, and Y. Li, "Copper catalyzing growth of single-walled carbon nanotubes on substrates," *Nano letters*, vol. 6, no. 12, pp. 2987–2990, 2006.
[17] S. Vollebregt, C. Beenakker, and R. Ishihara, "Carbon nanotubes as vertical interconnects in 3d integrated circuits," 2014.
[18] T. Iwasaki, G. Zhong, T. Aikawa, T. Yoshida, and H. Kawarada, "Direct evidence for root growth of vertically aligned single-walled carbon nanotubes by microwave plasma chemical vapor deposition," *The Journal of Physical Chemistry B*, vol. 109, no. 42, pp. 19 556–19 559, 2005.
[19] K. Gjerde, R. R. Kumar, K. N. Andersen, J. Kjelstrup-Hansen, K. B. Teo, W. I. Milne, C. Persson, K. Mølhave, H.-G. Rubahn, and P. Bøggild, "On the suitability of carbon nanotube forests as non-stick surfaces for nanomanipulation," *Soft Matter*, vol. 4, no. 3, pp. 392–399, 2008.

Nikolas Gaio received the B.S degree in electronic engineering from the Polytechnic University of Milan, Milan, Italy in 2012. In 2011 he was Visiting Student at Tongji University, Shanghai, China, where he received a B.Eng. in Electronic Information in 2013. In 2013, he joined as guest resercher the Shenzhen Institute of Advanced Technology (Chinese Academy of Science). In 2015 he received a M.Sc. (cum laude) in Biomedical Engineering in Delft University of Technology, the Netherlands. He is currently a PhD in the Department of Electronic Components, Technology and Materials (ECTM), Delft University of Technology, Delft, The Netherlands. His research focuses on Organ-on-chip and Microelectrode arrays. His areas of interests include design, microfabrication and characterization of MEMS devices. He received the Best Student Paper Award at the 2015 IEEE Sensors.

Cinzia Silvestri received the B.S degree and the M.Sc. degree (cum laude) in electronic engineering from the University of Roma Tor Vergata, Rome, Italy in 2009 and 2012, respectively. In 2011 she was Visiting Student at the Technical University of Munich, Munich, Germany. She is currently a PhD in the Department of Electronic Components, Technology and Materials (ECTM), Delft University of Technology, Delft, The Netherlands. Her research focuses on novel thermal management solutions for 3D heterogeneous integration, based on carbon related material (CNTs, graphene). Her areas of interests include design, microfabrication and characterization of MEMS devices as well as large-scale integration of 2-D materials. She received the Student Paper Competition Award - Track 1 at the 2014 IEEE Sensors.

Berend van Meer received his M.Sc. degree in micro electrical engineering from the Delft University of Technology, The Netherlands, in 2014. For his Masterfis thesis, he developed fabrication methods for Cytostretch Organ-on-Chip. He is currently pursuing his Ph.D degree within the department of Anatomy and Embryology at Leiden University Medical Center, The Netherlands, where he is working on developing a synthetic mimic for human myocardium based on stem cell derived cardiomyocytes.

Sten Vollebregt was born in Delft, The Netherlands, in 1984. He received his M.Sc. (cum laude) in Electrical Engineering in 2009, and PhD in Microelectronics in 2014, both from Delft University of Technology. During his PhD he worked on the application of carbon nanotubes as interconnects in 3D monolithic integrated circuits. Currently he is working as post-doc on the wafer-scale growth of graphene and its integration into semiconductor technology for sensing applications.

Christine Mummery is Professor of Developmental Biology and Chair of the Department of Anatomy and Embryology. She trained in Biophysics at London University and after her PhD was Royal Society postdoctoral fellow at the Hubrecht Institute in Utrecht, where she later became staff member and group leader. She became Professor at the Interuniversity Cardiology of the Netherlands (ICIN) at the University Medical Centre Utrecht in 2002. In 2007, she was a joint Harvard Stem Cell Institute/Radcliffe fellow at Harvard and Mass General Hospital at the time human induced pluripotent stem cells were being developed and was later the first to derive iPSC lines from patients in the Netherlands. Her primary research focus is currently the development and use of stem cells in cardiovascular development and disease. In 2008 she became Professor of Developmental Biology at the LUMC and Head of Department in 2009.. She is a member of the Royal Netherlands Academy of Arts and Sciences (KNAW), editor in chief of Stem Cell Reports and past president of the International Society of Differentiation. She received the Hugo van de Poelgeest Prize for animal alternatives in 2013, and the Hans Bloemendaal Medal in 2014.

Ronald Dekker received the M.Sc. degree (cum laude) in GaAs MESFET modeling from the Eindhoven University of Technology, Eindhoven, The Netherlands, and the Ph.D. degree (cum laude) in substrate transfer from the Delft University of Technology, Delft, The Netherlands, in 2004. He joined Philips Research, Eindhoven, The Netherlands, in 1988, where he worked on the development of RF technologies for mobile communication. In this context, he developed the concept of substrate transfer. From 2000 onward, his research has focused on flexible electronics and MEMS technology. Since 2007, he has been a part-time Professor with the Electronic Components, Technology and Materials Laboratory, Electrical Engineering Faculty, Delft University of Technology, Delft, The Netherlands. He has authored publications in leading journals and conference proceedings and holds 55 patents. Prof. Dekker was the recipient of the Philips Research Gilles Holst Peer Award in 2000.